Article

Modeling acoustic channel variability in underwater network simulators from real field experiment data

Filippo Campagnaro [1]*, Nicola Toffolo [1] and Michele Zorzi [1]

[1] Department of Information Engineering, University of Padova; {campagn1,toffolonic,zorzi}@dei.unipd.it
* Correspondence: campagn1@dei.unipd.it; Tel.: +39-049-827-7778

Version July 20, 2022 submitted to Electronics

Abstract: The underwater acoustic channel is remarkably dependent on the considered scenario and the environmental conditions. In fact, channel impairments differ significantly in shallow water with respect to deep water, and the presence of external factors such as snapping shrimps, bubbles, rain or ships passing nearby, changes of temperature and wind strength, can change drastically the link quality in different seasons and even during the same day. Legacy mathematical models that consider these factors exist, but are either not very accurate, like the Urick model, or very computationally demanding, like the Bellhop ray tracer. Deterministic models based on lookup tables (LUTs) of sea trial measurements are widely used by the research community to simulate the acoustic channel, in order to verify the functionalities of a network in certain water conditions before the actual deployment. These LUTs can characterize the link quality by observing, for instance, the average packet error rate or even a time varying packet error rate computed within a certain time window. While this procedure characterizes well the acoustic channel, the obtained simulation results are limited to a single channel realization, making it hard to fully evaluate the acoustic network in different conditions. In this paper, we discuss the development of a statistical channel model based on the analysis of real field experiment data, and compare its performance with the other channel models available in the DESERT Underwater network simulator.

Keywords: underwater acoustic channel; Hidden Markov Model; DESERT Underwater network simulations.

1. Introduction and Related Works

Wireless communication under the sea is very challenging. Radio frequency and optical signals are severely attenuated and therefore unable to cover a great distance, hence their use is restricted to a few specific applications [1]. Acoustic signals, instead, can propagate for several kilometers, and, while characterized by low bandwidth and high propagation delay, at least enable long range communication links, and are considered the most mature underwater wireless communication technology to date. For this reason, underwater acoustic networks (UANs) are widely used in both military and civilian applications, including, but not limited to, coastal surveillance and monitoring, tsunami prevention and oil and gas pipeline inspection. While sea trials are proven to be the best way to evaluate UANs, their realization is not trivial, in fact they are very demanding in terms of costs, time, personnel and equipment, and very prone to external factors that can cause failures of the trial, not only due to equipment issues caused by software faults and hardware damages, but also because of bad sea conditions. For this reason, network simulators are often employed for a preliminary evaluation, in order to debug the protocol stack before the final sea trial, hence minimizing the probability of software faults and having an idea on how the new protocol works if compared to other benchmarks. However, in the underwater research community simulations are still not considered to be a valuable tool to perform the final evaluation of UANs, as channel models are often unable to accurately describe the time varying behavior of a real acoustic channel [2]. The acoustic channel, in fact, depends on a large number of factors. First, changes of temperature, depth of the node and salinity cause a variation of the sound speed along the water column, and therefore of propagation of the acoustic signal Second, the presence of water currents, wind and mobile nodes causes a strong Doppler effect that affect the received signal [3]. Last, noise caused by wind waves, rain, snapping shrimps, bubbles brought by tidal inflow, and ship propellers [4] causes the degradation of the signal to noise ratio (SNR). The use of realistic channel models, such as the Bellhop ray tracer [5] where a subset of these parameters can be included, is computationally demanding and hence restricted to networks with a small number of nodes.

Given the large number of sea experiments performed by scientists in the last 15 years [6–10], a wide dataset of time-varying links has been collected, and some measurements are publicly available. Data-driven models have gradually been used to predict the trend of channel performance; for example, in [11] the authors, considering as features for the model different environmental characteristics, build a logistic regression network whose Packet Success Rate (PSR) estimates are quite accurate if restricted to the short-term variability of only one of the acoustic link features used to build the regression network. In several works [12–14] the authors mapped different modems performance figures of PSR versus range in the DESERT network simulator [15]. Although in some cases they have also included the performance degradation due to interference, this model can only be used for a preliminary evaluation of the network, as the channel variability is not considered and the modem performance is assumed constant in time. The ASUNA dataset [6] is a collection of the acoustic link quality time evolution observed during many different sea trials carried out by the Haifa University, Israel, the University of Padova, Italy, and IMDEA Networks, Spain. These experiment have been performed in different locations around Europe and Israel. The authors also show how the time varying links stored in the dataset can be used in a Matlab network simulation in order to reproduce the link quality evolution experienced during those sea trials. Similarly, in [16] the authors included in the DESERT Underwater network simulator the time evolution of the links of the multimodal acoustic mobile ad hoc network deployed in [9] and composed of low- and high-frequency modems. They also included the impairments caused by interference, and LUTs of the noise variability to test the adaptation of different modulation and coding schemes. Although, on the one hand, both the solutions in [6] and [16] allow to reproduce the time evolution observed during sea trials, on the other hand they do not allow to test different channel realizations.

During the last decade researchers [17,18] demonstrated that the time evolution of underwater acoustic channels can be statistically well characterized with two- and four-state Markov models and with a two-state Hidden Markov Model (HMM) [19]. In fact, the nature of the acoustic channel, whose error probability often changes during the day due to, for instance, presence of rain, changes of wind speed and shipping activity, can be well characterized by HMM. Analyzing real channel measurements [6–10], in fact, it is common to observe time intervals with a low PSR alternated by time intervals with a high PSR, rather than having an almost constant error probability during the whole experiment.

The evaluation study of which Markov and HMM model best fits the experimental data [18] showed that the HMM yields an accurate reproduction of the channel metrics, tracking well long term channel behaviors, and making it a good choice for modeling the channel in UANs simulators.

The aim of this work is to present a statistical model based on the analysis of sea trial data, and to evaluate the effectiveness of this model with respect to already existing models. This statistical model is included in the DESERT Underwater simulator [15], that includes a wide set of protocols for best customizing the underwater network to the needs of a user. The model relies on measurements extracted from the ASUNA dataset [20], that presents a number of time series of link quality indicators (LQIs), measured during the aforementioned experiments. The main contribution of this article is to provide the research community with an open-source framework for underwater network simulations where the acoustic channel is modeled with high reliability and low computation complexity.

The paper is structured as follows. First, in Section 2 we present the dataset used to infer the channel model parameters. Then, in Section 3 we provide the details of the statistical model and its implementation in the simulator. In Section 4 we evaluate the performance of our model when compared to legacy mathematical models, while in Section 5 we present the results of the simulations. Finally, in Section 6 we draw our concluding remarks.

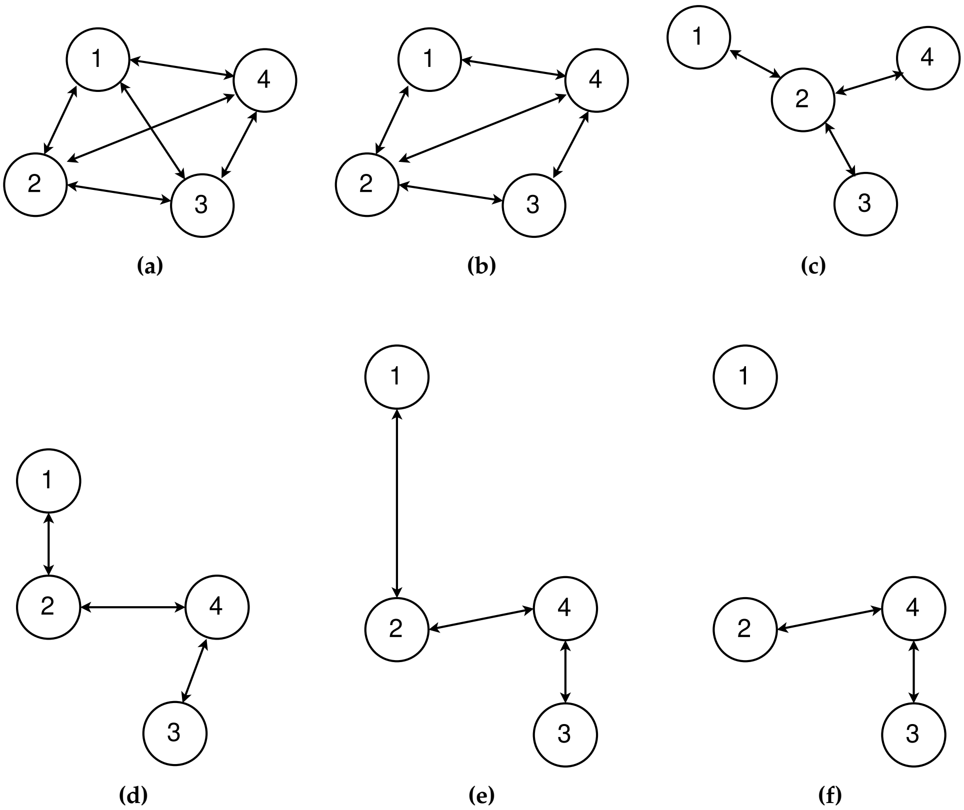

Figure 1. Topologies tested in the sea trial [6]: topology 1 (a), topology 2 (b), topology 3 (c), topology 4 (d), topology 5 (e), and topology 6 (f).

2. Dataset Description

The statistical model used in this paper is trained using the measurement data of one of the sea trials collected in the ASUNA dataset: the Haifa harbor (Israel) test performed in May 2009 [21]. During this experiment, 4 meter rubber boats deployed the nodes in six distinct topologies for different periods of time. A spatial reuse TDMA protocol (each device had a 5 second slot dedicated for transmission) was tested, and the transmission rate of the modems was 600 bps without channel coding, using a B-PSK signal modulated by direct sequence spread spectrum (DSSS), which was created using a gold sequence-based pseudo random sequence of 128 chips, centered at 25 kHz, and bandwidth 5 kHz. The modem prototype was composed of ITC transceivers, a National Instrument data acquisition system, and a laptop for signal processing. The transceivers were deployed at a depth of 4 m.

The LQI observed during the trial is the Bit Error Rate (BER), defined as the ratio between the number of erroneous bits and the total number of transmitted bits. The dataset provides a set of time-varying BER per-link values collected into six Topology Matrix Information (TMI) (one for topology). A TMI consists of an `NxN` matrix, with N the number of nodes in a topology, where the entry (t, i, j) represents the BER value for the link from node i (transmitter) to node j (receiver) at time t: the time interval between two subsequent measurements is 5 s, at each measurement BER and GPS position (in UTM coordinates) of each node are recorded. During the sea trial, Topology 1 was tested for 30 minutes, Topology 2, 3, 4 and 5 were tested for 60 minutes while topology 6 was tested for 90 minutes. Table 1 provides the experiment details.

Table 1. Haifa Harbor sea trial details

Location, Date	**Nodes**	**Topologies**	**Collection Time**
Haifa Harbor, 05/09	4	6	30-90 minutes
Rate	**LQI**	**Total Time**	**Interference**
Once every 5 s	BER	6 hours	No

During the experiment the LQI of each link was varied in time. In some of the links the BER was very small for almost all the time, while other links had a higher error rate.

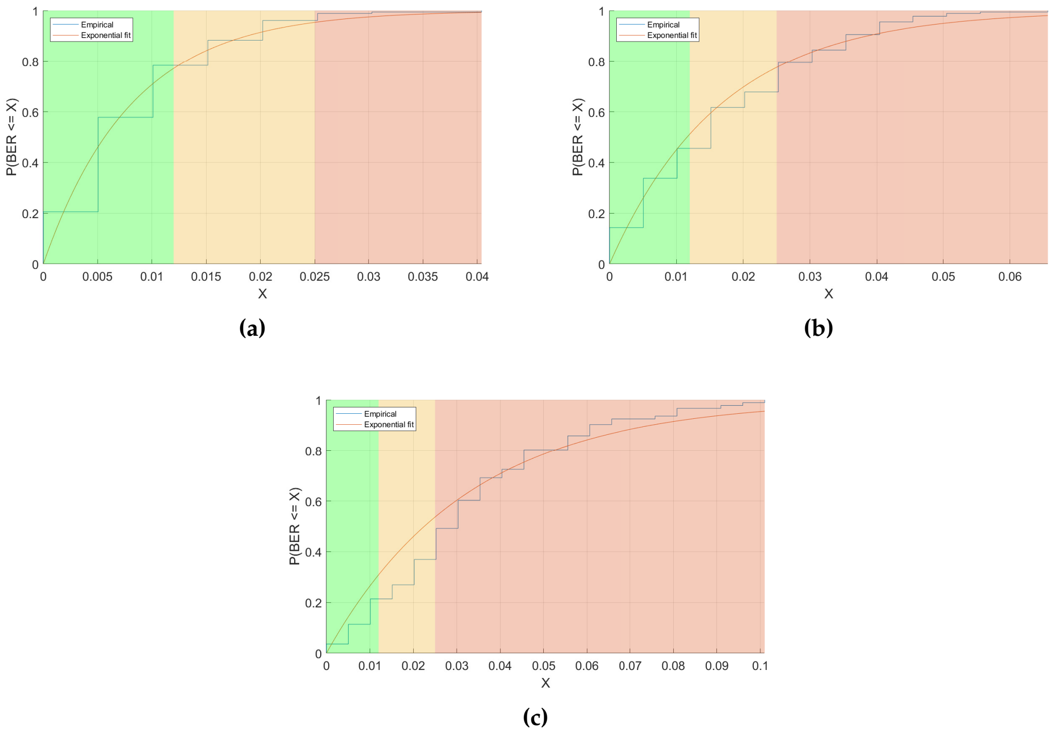

Figure 2. Examples of BER CDF fits for the stable link from node 4 to node 2 observed in topology 2 (a), the average link from node 3 to node 2 observed in topology 2 (b), and the challenging link from node 1 to node 3 observed in topology 1 (c).

For instance, in Figure 2 we can observe the BER Cumulative distribution function (CDF), fitted with an exponential distribution, of three representative links observed during the trial.

Specifically, Figure 2a presents the CDF of the very stable link from node 4 to node 2 observed in topology 2, whose BER is lower than 0.02 for 90% of the time. Figure 2b, instead, presents the CDF of the link from node 3 to node 2 observed in topology 2: in this case the BER is slightly higher than in the previous case but never exceeds 0.06. Finally, Figure 2c depicts the link from node 1 to node 3 observed in topology 3: this link has a BER that is definitely higher than the other two links.

3. Three-State Hidden-Markov Model

In this section we analyze the data measurements in order to obtain the statistic characterization of the acoustic channel experienced during the sea trial (Section 3.1) and compute the transition probabilities of the three-state HMM used to model the channel variability (Section 3.2). We also present the two-state HMM used as benchmark (Section 3.3). We analyze only the time evolution of the acoustic links of the nodes in communication range of each other, as nodes that are not in range simply did not exchange any message and their analysis is therefore trivial. Although the analysis presented in this paper focuses on topologies 1 and 2, in the new release of DESERT we also included the link evolution statistics of topologies 3, 4, 5 and 6.

3.1. BER Thresholds

In order to analyze the link quality, we need to define when a link is assumed to be in "good", "medium" and "bad" state. For this reason, we set the following thresholds to the observed BER:

- **Good state**: $BER < 0.012$;
- **Medium state**: $0.012 < BER < 0.025$;
- **Bad state**: $BER > 0.025$.

With these thresholds, considering a Hamming(7,4) Forward Error Correction (FEC) and a packet size of 16 bytes without FEC (i.e., 28 bytes with FEC), the resulting Packet Error Rate (PER) can be computed analytically as follows. If we define the probability of having no more than one error in 7 bits as

$$\mathbb{P}_{succ} = (1 - BER)^7 + 7 \cdot BER(1 - BER)^6, \tag{1}$$

we can obtain

$$PER = 1 - (\mathbb{P}_{succ})^{224/7}. \tag{2}$$

To check that these results are correct we verified them via simulation. Given a topology, a link and its empirical BER observed at a fixed time t_x, a sequence of 224 uniform random values in $[0, 1]$ are extracted. Each of the values has been compared with the respective BER empirical value to generate a logical array with "0" in the cells where the number generated by the RNG was greater than the BER value, and "1" in the other positions. This array can be interpreted as our 224 bit packet, where the bits set to "1" are wrong and the bits set to "0" are correct. Therefore, since we have adopted Hamming(7,4), the packet is scanned with a 7-bits step: since Hamming(7,4) cannot correct more than one error every 7 bits, whenever the sum of the bits in a block is greater than 1 we mark the block as compromised and the whole packet is considered corrupted. The process is iterated for $N = 1000$ times and the PER value is given by the number of corrupted packets divided by N.

We can observe in Figure 3 the PER-BER relationship obtained analytically (red line) and via simulation (blue crosses) for the three links presented in Figure 2.

With the BER thresholds presented above, the corresponding PER thresholds follow:

- **Good state**: $PER \leq 0.09$;
- **Medium state**: $0.09 < PER \leq 0.32$;
- **Bad state**: $PER > 0.32$.

We can finally observe that the stable link from node 4 to node 2 observed in topology 2 is 95% of the time in Good or Medium states, the average-performance link from node 3 to node 2 observed in topology 2 is only 80% of the time in Good or Medium states, and the challenging link from node 1 to node 3 observed in topology 1 is in Bad state 45% of the time.

With these fits, we can compute the generic probability that a link is in one of the three-states. Nevertheless, this is not enough to model the variability of the channels.

3.2. Transition Probabilities

From a visual inspection of the link BER time evolution we noted that, grouping the data on a per-state basis, a link in a state i is more likely to remain in that state in the successive time slot, rather than jump to another state. Once this was verified, we decided to model the PER time evolution of a generic link as a three-state Markov chain (Figure 4), with the three states $S = \{G, M, B\}$ that stand for

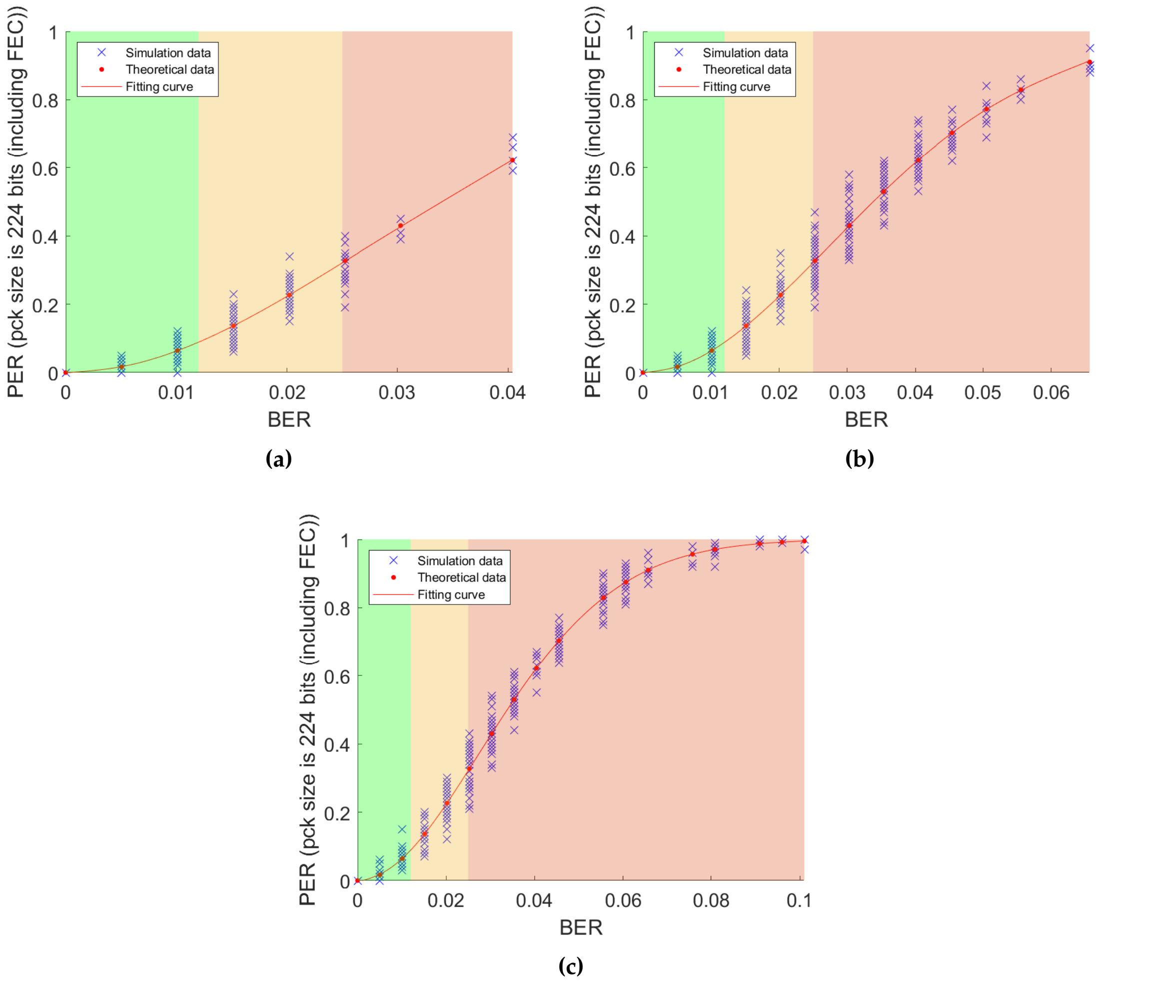

Figure 3. PER vs BER values considering a packet with 16 bytes payload and Hamming(7,4) FEC for three different links: the “Good" link from node 4 to node 2 observed in topology 2 (a), the “Medium" link from node 2 to node 2 observed in topology 2 (b), and the “Bad" link from node 1 to node 3 observed in topology 1.

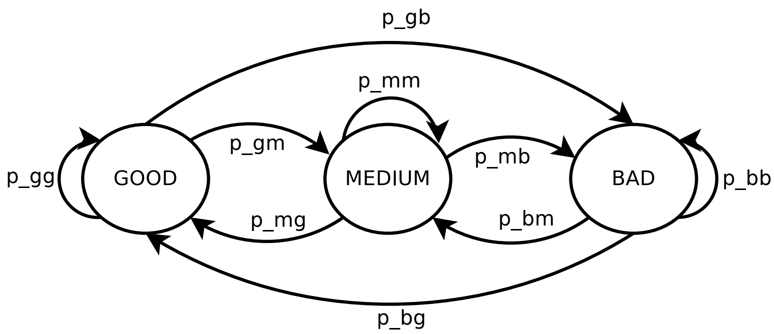

Figure 4. Three-state channel model.

“Good", “Medium", and “Bad", respectively. Specifically, if we denote as $X_0, \ldots, X_n, \ldots X_N$ a sequence of random variables where X_i takes values in the set S of the three states, $\mathbb{P}(X_{n+1} = j | X_n = i)$ is the *transition probability* from state i to state j at step n. Additionally, by the Markov property, we have that:

$$\mathbb{P}(X_{n+1} = i_{n+1} | X_0 = i_0, \ldots, X_n = i_n) = \mathbb{P}(X_{n+1} = i_{n+1} | X_n = i_n), \tag{3}$$

which can be interpreted as the fact that, if the current state $X_n = i_n$ is known, the probability of $\mathbb{P}(X_{n+1} = i_{n+1})$ does not depend on the previous states. If the transition probabilities do not depend on n but only on i and j, the Markov chain is *homogeneous* and we may compute every joint probability knowing only the initial distribution of the states $p_i^{(0)} = \mathbb{P}(X_0 = i)$ and the values of p_{ij}, where:

$$p_{ij} = \mathbb{P}(X_{n+1} = j | X_n = i), \forall n. \tag{4}$$

Exploiting matrix calculus, since we knew the frequencies of the BER values of each link, we found the *transition matrices* $P = (p_{ij})$, which have only non negative elements, are row-normalized to 1 and, in our case, have a size 3x3. In Figure 5 we show the matrix charts presenting the transition matrices for the three links discussed so far.

A relevant result is that, given the transition matrix P^n at time n, it is possible to compute the t-step transition probabilities by means of matrix exponentiation:

$$\mathbb{P}(X_{n+t} = j | X_n = i) = (P^t)_{ij}, \forall n \geq 0. \tag{5}$$

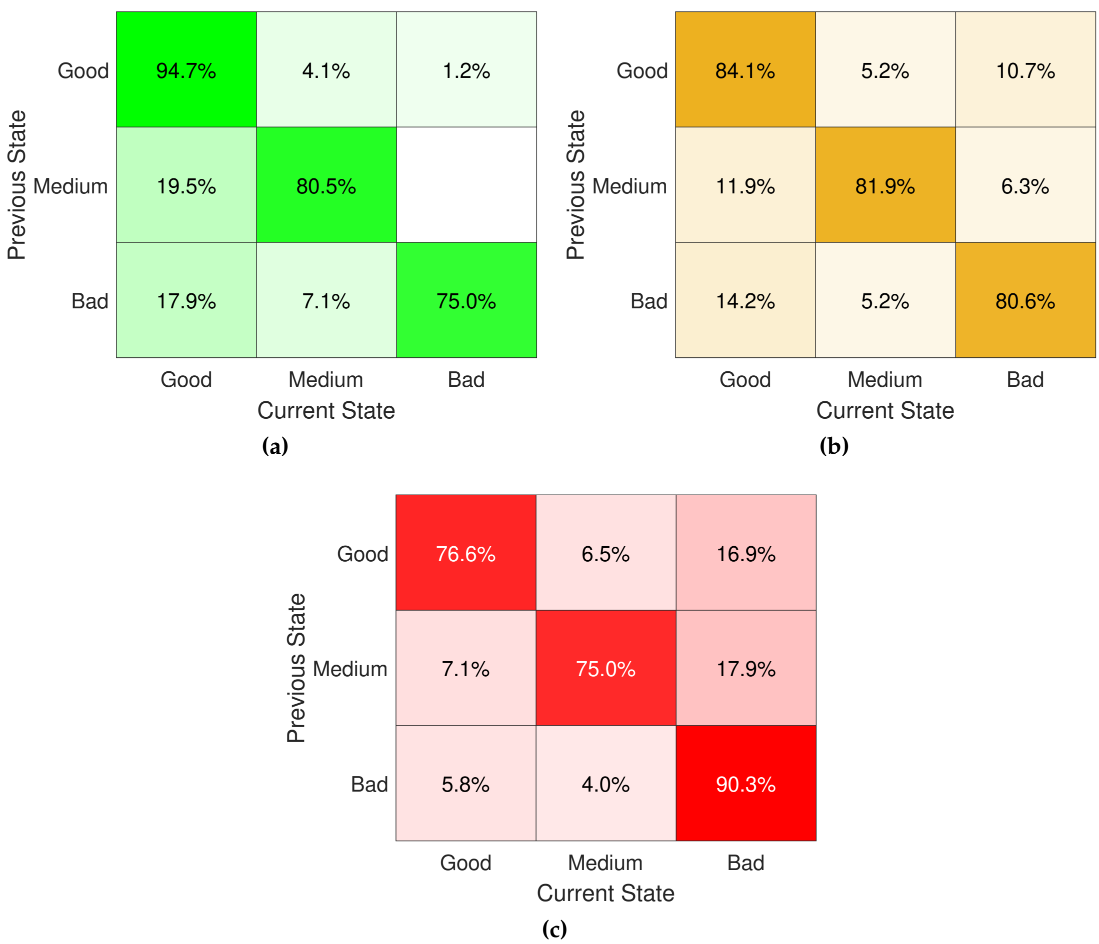

Figure 5. Examples of transition matrices: transition matrix P of the links from node 4 to node 2 observed in topology 2 (a), from node 3 to node 2 observed in topology 2 (b), and from node 1 to node 3 observed in topology 1 (c).

The averaged values of the BER in the three states for the links we are considering are reported in Table 2.

Table 2. Average BER values, three-state HMM

	avg good	**avg medium**	**avg bad**
Topology 2, link 4→2	0.0051	0.0174	0.0281
Topology 2, link 3→2	0.0048	0.0165	0.0338
Topology 1, link 1→3	0.0066	0.0184	0.0448

3.3. Two-State Hidden-Markov Model

As benchmark of the three-state HMM presented in Section 3, we now present the more used two-state HMM (Figure 6).

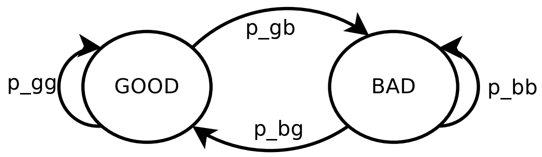

Figure 6. Two-state channel model.

In the two-state model, we define a cumulative Bad state b' grouping together the Bad and the Medium states used in the three-state model. The probabilities of successful reception given a channel state are computed link-wise by taking the average PERs in each state. The transition probabilities, instead, are computed starting from the three-state model transition probabilities as:

- $p_{gb'} = 1 - p_{gg}$,
- $p_{b'g} = \frac{p_{mg} \cdot p_m + p_{bg} \cdot p_b}{1 - p_g}$,
- $p_{b'b'} = 1 - p_{b'g}$,

where p_{gg} is the probability of not having a transition at time $n+1$ when a link is in the Good state at step n for the three-state HMM and $p_s, s \in \{g, m, b\}$ is the generic probability a link finds itself in the Good, Medium or Bad state respectively.

While with the three-state HMM the transition matrix P^n at step n needs to be computed with matrix exponentiation as presented in eq. (5), in the simple two-state model the transition probabilities at step n can be obtained via the closed formula [22]:

$$P^n = \frac{1}{p_{gb'} + p_{b'g}} \begin{pmatrix} p_{b'g} & p_{gb'} \\ p_{b'g} & p_{gb'} \end{pmatrix} + \frac{(1 - p_{gb'} - p_{b'g})^n}{p_{gb'} + p_{b'g}} \begin{pmatrix} p_{gb'} & -p_{gb'} \\ -p_{b'g} & p_{b'g} \end{pmatrix}. \tag{6}$$

In Figure 7 we report the transition matrices in the two-state HMM for the links under analysis. Table 3 shows the relevant averaged BER values for the two-state HMM.

Table 3. Average BER values, two-state HMM

	avg good	**avg bad**
Topology 2, link 4→2	0.0051	0.0193
Topology 2, link 3→2	0.0048	0.0267
Topology 1, link 1→3	0.0066	0.0395

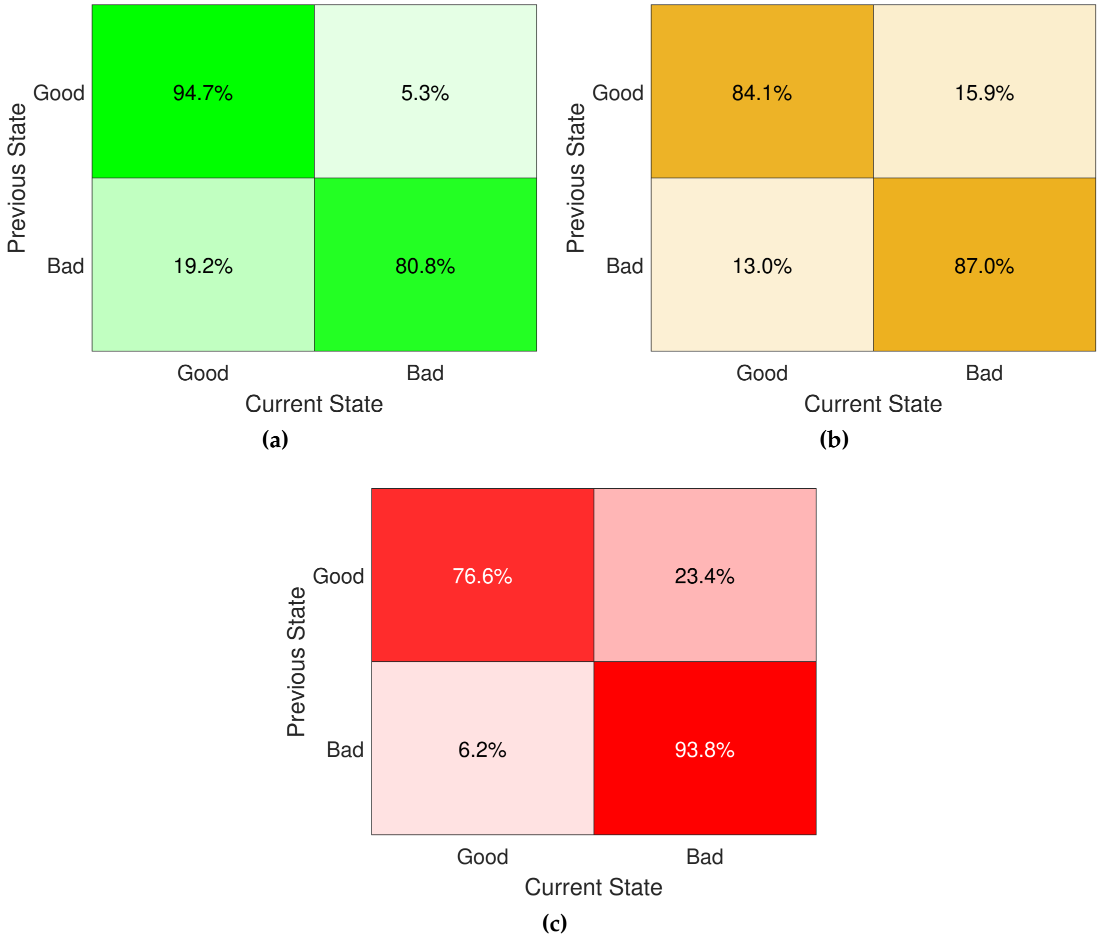

Figure 7. Examples of transition matrices for the two-state HMM: transition matrix P of the links from node 4 to node 2 observed in topology 2 (a), from node 3 to node 2 observed in topology 2 (b), and from node 1 to node 3 observed in topology 1 (c).

4. Model Implementation and Simulation

In order to evaluate the models presented in the previous sections, we implemented the two- and three-state HMM in the DESERT Underwater framework [15], an open-source underwater network simulation and experimentation tool publicly available in [23]. Notably, the DESERT Underwater legacy physical module, called UWPhysical, models the path-loss with the Urick and Thorp formulas, and computes the signal to noise ratio using the model presented in [2]. Although this model is largely used by researchers, it does not address well the variability of the acoustic channel. Therefore, we implemented from scratch two new physical layers, one called UWHMMPhysical that uses the two-state HMM described in Section 3.3, and one named UWHMMPhysicalExtended that uses the three-state HMM presented in Section 3. In both physical layers we included the statistics of each link using the so called `link-stats` objects, and let the physical layer compute the probability that a packet is correctly received at a specific moment, hence providing a per-link channel variability. The `link-stats` objects are independent of each other: in the case of near nodes that share the same channel, the same `link-stats` object can be used to model the channel variability in the same way: in the case of the sea experiment considered in these simulations, the links between the nodes are considered independent, hence a different `link-stats` object is used to model the channel variability between every pair of nodes.

The most relevant difference between the two- and three-state HMM is the way the transition probabilities are computed. As explained in Section 3.3, the two-state HMM can be computed via a closed formula, while for the three-state HMM the transition probability can only be computed by means of matrix exponentiation. This implies that the exponentiation has to be performed efficiently, so that even with a big exponent n, the complexity is limited and not growing without bounds. Given that n monotonically increases during the simulation, it is not necessary to compute P^n starting from the initial transition matrix P^0, as this would cause a degradation in performance. Specifically, we save the aforementioned matrix each time we compute it, so that we can operate conveniently on the last available P^k and compute P^n with a number of exponentiations equal to $n-k$, that is strictly less than n. As a result, the computation time of a simulation using the three-state model is not much longer than the same simulation relying on the legacy physical model or on the two-state HMM.

4.1. Simulation Settings

In our simulations we analyze the system behavior with the nodes placed in the positions presented in topology 1 (Figure 1a) and topology 2 (Figure 1b). The simulation lasted 18000 s, and we switched from topology 2 to topology 1 in the middle of the simulation (i.e., at time 9000 s) by adding the link from node 1 to node 3 and changing the packet success probability per link and the transition probabilities of every link accordingly. The behavior of the three communication stacks depicted in Figure 8 is analyzed. All stacks use a constant bitrate application layer, static routing with all nodes transmitting to their 1-hop neighbors and a time division multiple access (TDMA) MAC layer. The first stack (Figure 8a) uses the legacy DESERT physical layer, the second stack (Figure 8b) uses the two-state HMM-based physical layer and, finally, the third stack (Figure 8c) employs the three-state HMM-based physical layer.

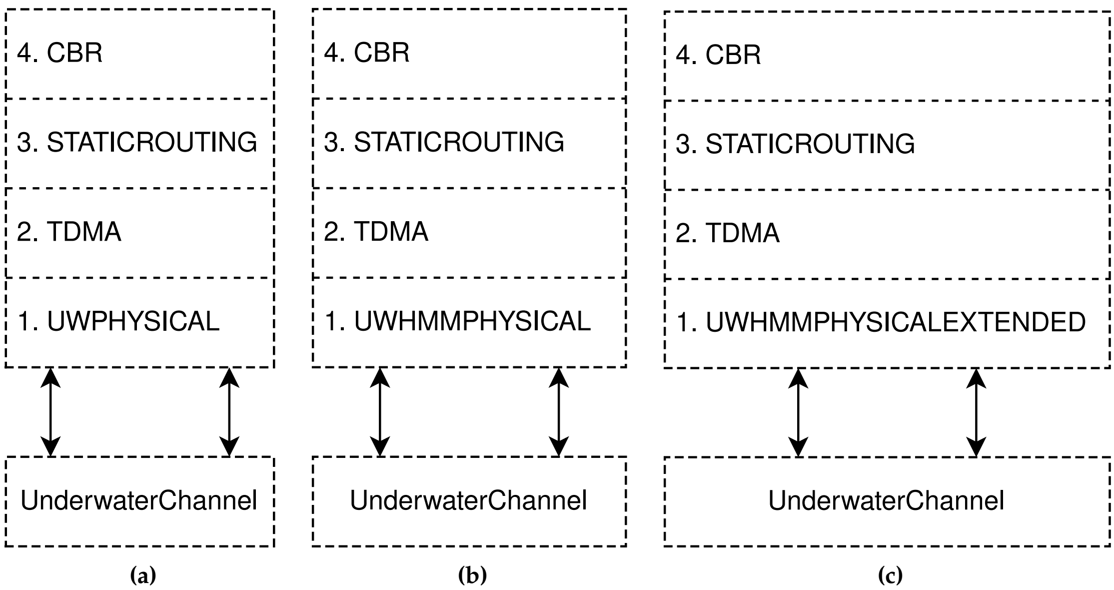

Figure 8. The three communication stacks compared in simulation, all composed of a constant bitrate application layer, static routing, and TDMA, and a different physical layer: `Uwphysical` (a), `UWHMMPhysical` (b) and `UWHMMPhysicalExt` (c).

The network is composed of 4 nodes and each node generates 28 bytes packets every 60 s. Bandwidth and carrier frequency are set to 5 kHz and 25 kHz, respectively, in order to best simulate the behavior of the modems used in the field experiment presented in Section 2. The simulation parameters are summarized in Table. 4.

The TDMA MAC is configured with a frame duration of 8 s, equally divided between the four nodes that have a time slot of 2 s each to transmit their packets. A guard time of 0.8 s is used to avoid interference caused by the propagation time and to consider possible synchronization errors between the nodes.

Table 4. Simulation parameters

Nodes	Pkt Size	Tx Duration	Tx Power
4	28 B	18000 s	165 dB
Frequency	**Bandwidth**	**Bitrate**	**Cbr Period**
25 kHz	5 kHz	600 bps	60 s

At the end of the simulations we observed the performance of each link of the network by computing PER and throughput averaging over 50 simulation runs and presenting the 95% confidence interval (CI).

5. Simulation Results

PER and throughput of each link are presented in Figures 9 and 10, respectively. Figure 9 compares the PER per link obtained with the three physical layers described in Section 4.1 with the PER measured during the sea trial (green diamond). Uwphysical (Figure 9a) is extremely optimistic and provides

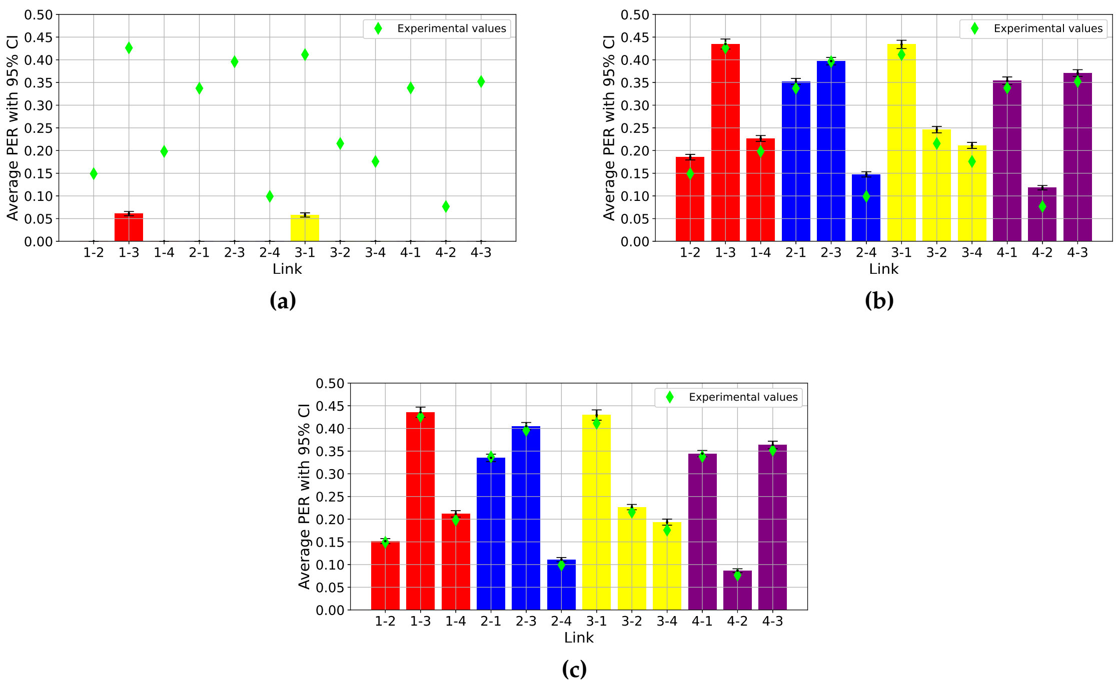

Figure 9. PER results yielded by the simulations (bars) with respect to Haifa Harbor measurements (green diamond) for `UWPhysical` (a), `UWHMMPhysical` (b) and `UWHMMPhysicalExt` (c).

a very low PER. In particular, with the considered settings the PER of the links is equal to zero up to a transmission range of 1.1 km, and increases to 1 when the distance between nodes is more than 1.6 km. This implies that the link connecting the two farthest nodes (node 1 and node 3, that are 1.2 km from each other) has a non-zero PER, but still the real values are underestimated. Conversely, the PER obtained both with the two-state (Figure 9b) and with the three-state (Figure 9c) models is very similar to the one observed in the sea trial, with the three-state model having a PER that matches almost perfectly (within the CI) the experimental one (depicted with green diamonds), definitely outperforming the other two models.

Similarly, the throughput observed with Uwphysical (Figure 10a) is almost the same for all of the links, and is equal to 3.7 bps: only in the link between node 1 and 3 the throughput is approximately 1.85 bps, as that link was removed at the simulation time 9000 s, when the network topology was changed from topology 1 to topology 2. With a higher PER per link, the throughput observed with the two- and three-state HMM is significantly different link by link, presenting results that are definitely closer to those that can be observed during a sea experiment.

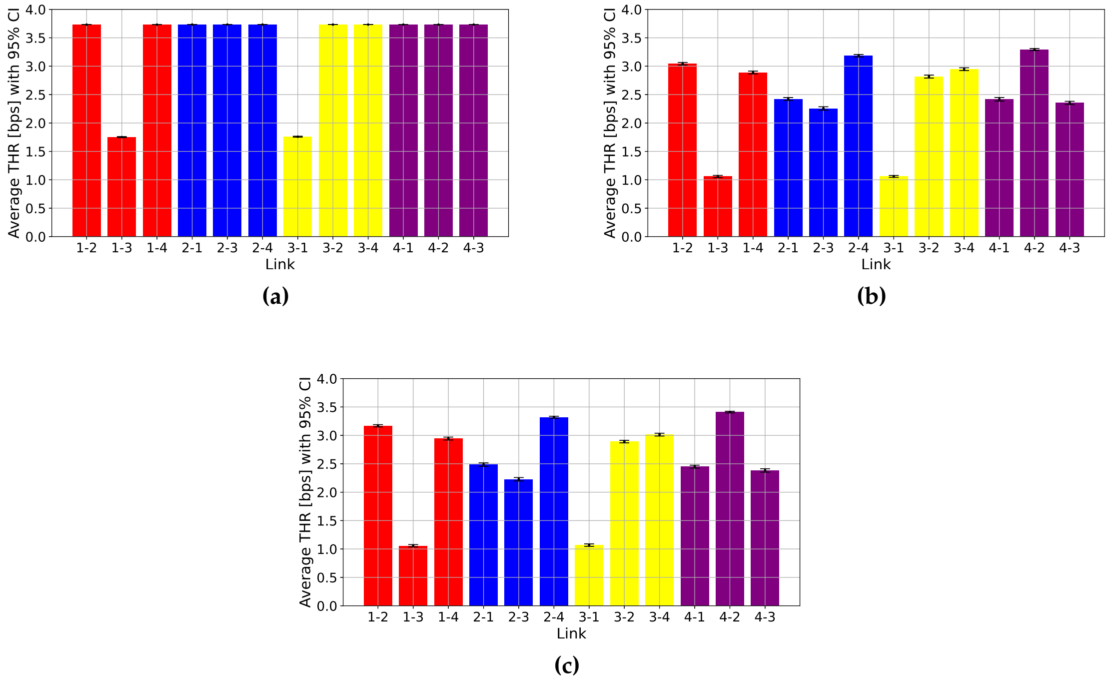

Figure 10. THR results yielded by the simulations with respect to Haifa Harbor measurements for `UWPhysical` (a), `UWHMMPhysical` (b) and `UWHMMPhysicalExt` (c).

Finally, we report some plots showing the variability of throughput in time (i.e., computed every 300 seconds) for the links from node 4 to node 2 and from node 1 to node 3, and again we see how optimistic the results obtained using the simplest PHY module are. We can observe the jump at 9000s for the link $1 \rightarrow 3$, due to the switch from topology 2 (where the link was not in place) to topology 1. Besides, the values for the throughput are constant for the UWPhysical module, but for the links $1 \rightarrow 3$ and $3 \rightarrow 1$, which are the only ones having a PER greater than zero. Conversely, the throughput obtained with the two HMMs models is definitely lower, due to the higher PER, and has a higher variance, well characterizing the channel variability. While we could directly compare the PER obtained in simulation with that experienced during the experiment, we could not perform the same operation for the throughput, as the simulation used an application layer generating traffic with different rate than the one used during the sea trial. This tool can be used to test protocol stack configurations that are different from the one used in the experiment, exploiting the measures obtained during the sea trial to model the packet error rate time evolution and observing as a result other performance indicators, such as the throughput per link.

6. Conclusions

In this paper we presented two statistical models to characterize the underwater acoustic channel in network simulators, matching well the results observed during sea trials. Specifically, we were able to develop two precise channel models for underwater communications starting from the analysis of real field experiment data retrieved from ASUNA. The models are based on two- and three-state Markov chains and have two main advantages: first, they guarantee a realistic channel modelling with respect to the results observed during sea trials; second, they are not particularly computationally demanding. Indeed, while for the two-state HMM the PER can be simply computed with a closed

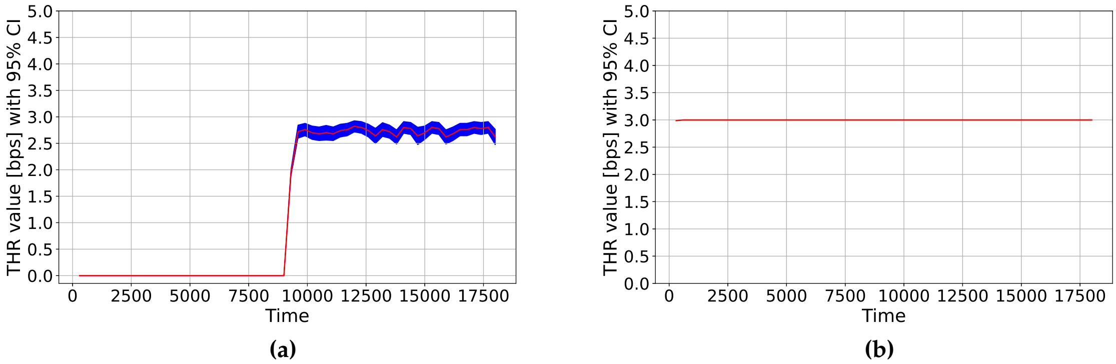

Figure 11. “Instantaneous" throughput values yielded by `UWPhysical` module from node 1 to node 3 (a) and from node 4 to node 2 (b).

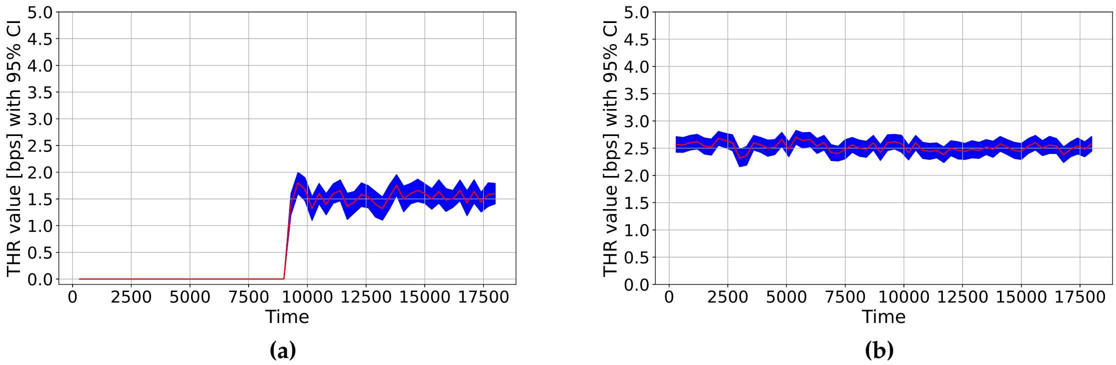

Figure 12. "Instantaneous" throughput values yielded by `UWHMMPhysical` module from node 1 to node 3 (a) and from node 4 to node 2 (b).

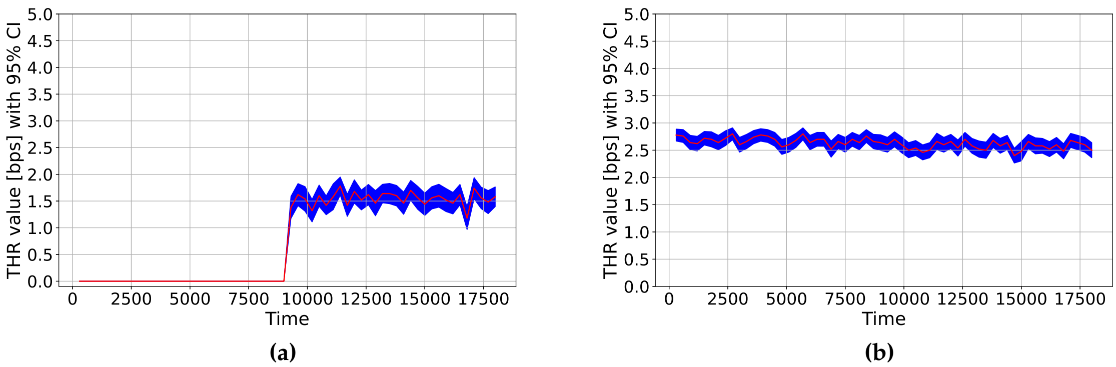

Figure 13. "Instantaneous" throughput values yielded by `UWHMMPhysicalExtended` module from node 1 to node 3 (a) and from node 4 to node 2 (b).

formula, for the three-state HMM the PER can be computed iteratively, starting from the last PER computed during the ongoing simulation. The two models revealed themselves to be adaptable to multiple configurations and flexible. Furthermore, they have both been extensively tested after having been implemented in the DESERT simulator and they have been compared with the existing legacy channel model already available in the simulator. The performance obtained with the two models were solid and proved their reliability, with the three-state HMM slightly outperforming the two-state

HMM, at the cost of a small increase in complexity. Possible future work may consist in investigating models with an increased number of states (i.e., more than 3), and to study the tradeoff given by the increased computational requirements and the fidelity of the results. Another aspect that deserves a specific investigation is how this channel model can be applied to mobile networks, e.g., by extending the number of states or including a penalty factor due to distance, speed and acceleration. This aspect is not trivial as the increase of a node speed does not cause only a strong Doppler effect, but also a strong acoustic noise caused by propellers and engine [24].

Author Contributions: conceptualization, Filippo Campagnaro and Nicola Toffolo; methodology, Nicola Toffolo and Filippo Campagnaro; data curation, Nicola Toffolo; investigation, Filippo Campagnaro; formal analysis, Nicola Toffolo and Filippo Campagnaro; software, Nicola Toffolo; validation, Filippo Campagnaro; writing–original draft preparation, Filippo Campagnaro; supervision, Michele Zorzi; resources, Michele Zorzi; visualization, Nicola Toffolo and Filippo Campagnaro; project administration, Filippo Campagnaro and Michele Zorzi; funding acquisition, Filippo Campagnaro and Michele Zorzi.

Acknowledgments: This work has been partially supported by the European Union - FSE REACT EU, PON Research and Innovation 2014-2020 (DM 1062/2021).

References

1. Campagnaro, F.; Signori, A.; Zorzi, M. Wireless Remote Control for Underwater Vehicles. *Journal of Marine Science and Engineering* **2020**, *8*. doi:10.3390/jmse8100736.
2. Stojanovic, M. On the relationship between capacity and distance in an underwater acoustic communication channel. *ACM SIGMOBILE Mobile Computing and Communications Review* **2007**, *11*, 34–43.
3. Chitre, M.; Topor, I.; Bhatnagar, R.; Pallayil, V. Variability in link performance of an underwater acoustic network. MTS/IEEE OCEANS - Bergen, 2013. doi:10.1109/OCEANS-Bergen.2013.6607953.
4. Chitre, M.; Koay, T.B.; Deane, G.; Chua, G. Variability in Shallow Water Communication Performance Near a Busy Shipping Lane. Fifth Underwater Communications and Networking Conference (UComms), 2021. doi:10.1109/UComms50339.2021.9598017.
5. M. Porter *et al.*. Bellhop code. Last time accessed: Apr. 2022.
6. Casari, P.; Campagnaro, F.; Dubrovinskaya, E.; Francescon, R.; Dagan, A.; Dahan, S.; Zorzi, M.; Diamant, R. ASUNA: A Topology Data Set for Underwater Network Emulation. *IEEE J. Oceanic Engineering* **2021**, *46*, 307–318.
7. Tomasi, B.; Casari, P.; Zorzi, M.; Zappa, G.; McCoy, K. Experimental study of the acoustic channel properties during SubNet 2009. Technical report, University of Padova, 2010.
8. Tomasi, B.; Preisig, J.; Michele, M. On the predictability of underwater acoustic communications performance: The KAM11 data set as a case study. Proc. International Conference on Underwater Networks & Systems (WUWNet); , 2011.
9. van Walree, P.; Colin, M. In-situ performance prediction of a coherent acoustic modem in a reverberant environment. *IEEE Journal Oceanic Engineering* **2021**. accepted.
10. Otnes, R.; van Walree, P.A.; Buen, H.; Song, H. Underwater Acoustic Network Simulation With Lookup Tables From Physical-Layer Replay. *IEEE Journal Oceanic Engineering* **2015**, *40*, 822–840.
11. Kalaiarasu, V.; Vishnu, H.; Mahmood, A.; Chitre, M. Predicting underwater acoustic network variability using machine learning techniques. OCEANS 2017 - Anchorage, 2017.
12. Tapparello, C.; Casari, P.; Toso, G.; Calabrese, I.; Otnes, R.; van Walree, P.; Goetz, M.; Nissen, I.; Zorzi, M. Performance Evaluation of Forwarding Protocols for the RACUN Network; Association for Computing Machinery: New York, NY, USA, 2013; WUWNet '13. doi:10.1145/2532378.2532401.
13. Signori, A.; Campagnaro, F.; Steinmetz, F.; Renner, B.C.; Zorzi, M. Data Gathering from a Multimodal Dense Underwater Acoustic Sensor Network Deployed in Shallow Fresh Water Scenarios. *Journal of Sensor and Actuator Networks* **2019**, *8*. doi:10.3390/jsan8040055.
14. Campagnaro, F.; Favaro, F.; Casari, P.; Zorzi, M. On the feasibility of fully wireless remote control for underwater vehicles. 2014 48th Asilomar Conference on Signals, Systems and Computers, 2014, pp. 33–38. doi:10.1109/ACSSC.2014.7094391.
15. Campagnaro, F.; others. The DESERT Underwater Framework v2: Improved Capabilities and Extension Tools. Proc. Ucomms; , 2016.

16. Campagnaro, F.; Signori, A.; Otnes, R.; Goetz, M.; Sotnik, D.; Komulainen, A.; Nissen, I.; Favaro, F.; Guerra, F.; Zorzi, M. A Simulation Framework for Smart Adaptive Long- and Short-range Acoustic Networks. Proc. MTS/IEEE Oceans; , 2021.
17. Pignieri, F.; De Rango, F.; Veltri, F.; Marano, S. Markovian approach to model Underwater Acoustic channel: Techniques comparison. IEEE Military Communications Conference (MILCOM 2008), 2008. doi:10.1109/MILCOM.2008.4753161.
18. Tomasi, B.; Casari, P.; Finesso, L.; Zappa, G.; McCoy, K.; Zorzi, M. On modeling JANUS packet errors over a shallow water acoustic channel using Markov and hidden Markov models. IEEE Military Communications Conference (MILCOM 2010), 2010, pp. 2406–2411. doi:10.1109/MILCOM.2010.5680327.
19. Turin, W.; van Nobelen, R. Hidden Markov Modeling of Flat Fading Channels. *IEEE Journal on Selected Areas in Communications* **1998**, *16*, 1809–1817.
20. A Shared Underwater Network emulAtion dataset. https://sites.google.com/marsci.haifa.ac.il/asuna/. Last time accessed: Apr. 2022.
21. Diamant, R.; Shirazi, G.N.; Lampe, L. Robust Spatial Reuse Scheduling in Underwater Acoustic Communication Networks. *IEEE J. Ocean. Eng.* **2014**, *39*, 32–46.
22. Taylor, H.M.; Karlin, S. *An Introduction to Stochastic Modeling*, third ed.; Academic Press, 1999.
23. DEsign, Simulate, Emulate and Realize Test-beds for Underwater network protocols. http://desert-underwater.dei.unipd.it/. Last time accessed: Apr. 2022.
24. Coccolo, E.; Campagnaro, F.; Signori, A.; Favaro, F.; Zorzi, M. Implementation of AUV and Ship Noise for Link Quality Evaluation in the DESERT Underwater Framework. Proc. ACM WUWNet; , 2018.

© 2022 by the authors. Submitted to *Electronics* for possible open access publication under the terms and conditions of the Creative Commons Attribution (CC BY) license (http://creativecommons.org/licenses/by/4.0/).